



Strongly enhanced bacterial bioluminescence with the *ilux* operon for single-cell imaging

Carola Gregor^{a,1}, Klaus C. Gwosch^a, Steffen J. Sahl^a, and Stefan W. Hell^{a,b,1}

^aDepartment of NanoBiophotonics, Max Planck Institute for Biophysical Chemistry, 37077 Göttingen, Germany; and ^bDepartment of Optical Nanoscopy, Max Planck Institute for Medical Research, 69120 Heidelberg, Germany

Contributed by Stefan W. Hell, December 8, 2017 (sent for review September 12, 2017; reviewed by David W. Piston and Alice Y. Ting)

Bioluminescence imaging of single cells is often complicated by the requirement of exogenous luciferins that can be poorly cell-permeable or produce high background signal. Bacterial bioluminescence is unique in that it uses reduced flavin mononucleotide as a luciferin, which is abundant in all cells, making this system purely genetically encodable by the *lux* operon. Unfortunately, the use of bacterial bioluminescence has been limited by its low brightness compared with other luciferases. Here, we report the generation of an improved *lux* operon named *ilux* with an approximately sevenfold increased brightness when expressed in *Escherichia coli*; *ilux* can be used to image single *E. coli* cells with enhanced spatiotemporal resolution over several days. In addition, since only metabolically active cells produce bioluminescent signal, we show that *ilux* can be used to observe the effect of different antibiotics on cell viability on the single-cell level.

bioluminescence | luciferase | antibiotics | bacteria | microscopy

Bioluminescent cells generate light by a chemical reaction. The bioluminescence reaction is catalyzed by an enzyme called luciferase, with a luciferin required as substrate. Molecules of luciferin are converted into a product in an electronically excited state and emit a photon on return to the ground state, with visible light emitted in the process. There are many different luciferases and corresponding luciferins found in nature, indicating that bioluminescence has evolved more than 40 times independently during evolution (1), although in several cases, its biological function remains not fully understood. Most luciferins are only produced by organisms that express the corresponding luciferase, with the exception of the bacterial luciferin FMNH₂, reduced flavin mononucleotide (FMN), which is abundant in all cells.

The bacterial bioluminescence reaction is catalyzed by an αβ-heterodimeric luciferase coded by the genes *luxA* and *luxB*. In addition to FMNH₂, the luciferase binds molecular oxygen and a long-chain fatty aldehyde. The fatty aldehyde is oxidized to the corresponding fatty acid, and FMNH₂ is oxidized to FMN, thereby emitting a blue photon with a wavelength around the spectral emission maximum λ_{max} of ~490 nm:



To keep this reaction ongoing, the fatty aldehyde must be continuously regenerated. This is performed by the fatty acid reductase complex, which consists of a fatty acid reductase, trans-ferase, and synthetase coded by *luxC*, *luxD*, and *luxE*, respectively. Since an FMN reductase that generates FMNH₂ is present in *Escherichia coli*, introduction of the *luxCDABE* operon is sufficient to produce a bioluminescence output in these cells.

Due to its very low light levels compared with fluorescence, bioluminescence imaging is not routinely applied so far. However, bioluminescence provides several benefits compared with fluorescence measurements. First, there is virtually no background because of the lack of autofluorescence. Bioluminescence background levels in living cells are extremely low, making bioluminescence up to 50 times more sensitive than fluorescence (ref. 2 and references therein). Second, no excitation light source and

filters are required, making the setup very simple. In addition, it is possible to study processes where the intense excitation light required for fluorescence measurements would be disturbing, such as circadian rhythms or Ca²⁺ activity in the retina (3, 4). Third, no phototoxicity or bleaching occurs, allowing image acquisition over arbitrary timespans. Furthermore, bioluminescence is dependent on metabolic energy, and hence, only metabolically active cells are visible, preventing artifacts due to the observation of severely damaged or dead cells.

In addition to the limitation by their low brightness, the luciferases that are most commonly used exhibit several drawbacks, as the luciferin must be externally supplied. Limited solubility, stability, or cell permeability of the luciferin may, in some cases, hamper its usability (5–7). Administering of excess amounts of the luciferin is readily done for standard single-layered cell cultures, but luciferin consumption within larger collections of cells, such as tumors, is more rapid. In these situations, the luciferin concentration is not constant over time, and the signal decays sometimes within minutes (8, 9). Therefore, the luciferin has to be applied repeatedly for long-term imaging, which complicates quantification of the signal. Moreover, autooxidation of coelenterazine, the substrate of commonly used *Renilla* and *Gaussia* luciferase, can produce luminescence background signal (6, 10). Bacterial luciferase is the only luciferase to circumvent all of these problems, since FMN is present in all cell types and can be converted into free FMNH₂ by additional expression of an FMN reductase. Its main limitation is the poor brightness that is several orders of magnitude lower than that of other luciferases (11). Several attempts have been made to improve the brightness of bacterial bioluminescence, including splitting the *lux* operon for enhanced expression, codon optimization and additional expression of an

Significance

The emission of light generated in a process referred to as bioluminescence can be used for imaging of living cells over long timespans without phototoxicity or bleaching. The amounts of light produced in the bioluminescence process are very low, and exogenous substrate molecules are often required. We improved the brightness of bacterial bioluminescence, a system that features the advantage that all of the required molecular components are genetically encoded within a single operon. Consequently, we have engineered an improved operon *ilux*, which enables long-term visualization of single bacterial cells while simultaneously providing information about cellular viability.

Author contributions: C.G. and S.W.H. designed research; C.G. performed research; K.C.G. contributed new reagents/analytic tools; C.G. analyzed data; and C.G., S.J.S., and S.W.H. wrote the paper.

Reviewers: D.W.P., Washington University in St. Louis; and A.Y.T., Stanford University.

The authors declare no conflict of interest.

This open access article is distributed under [Creative Commons Attribution-NonCommercial-NoDerivatives License 4.0 \(CC BY-NC-ND\)](https://creativecommons.org/licenses/by-nc-nd/4.0/).

¹To whom correspondence may be addressed. Email: cgregor@mpibpc.mpg.de or shell@mpibpc.mpg.de.

This article contains supporting information online at www.pnas.org/lookup/suppl/doi:10.1073/pnas.1715946115/-DCSupplemental.

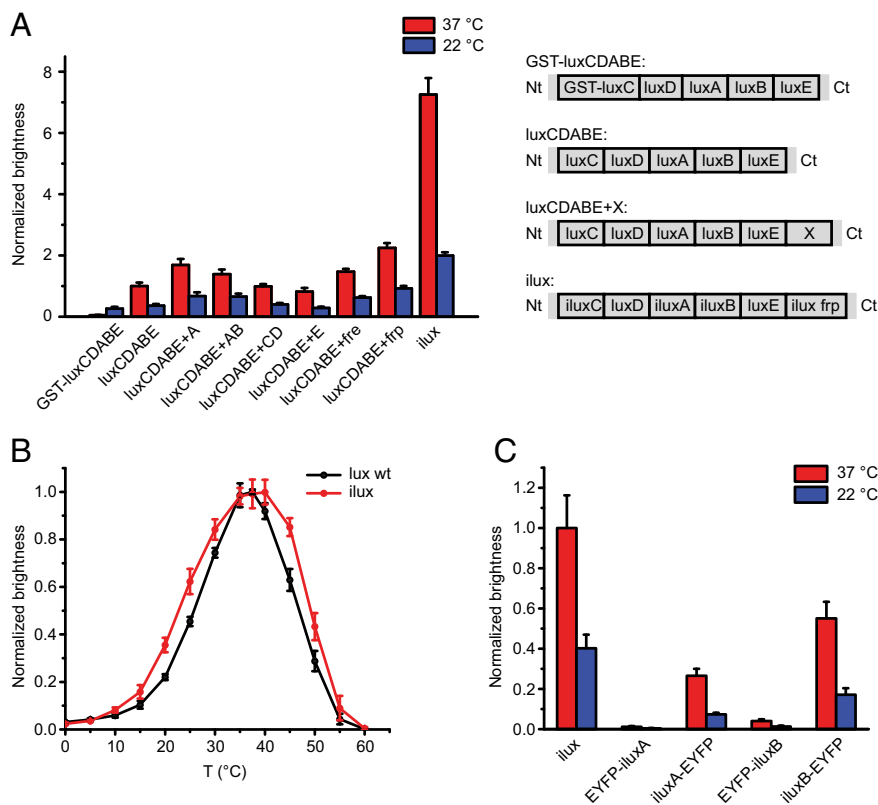


Fig. 1. Generation and comparison of *lux* variants with increased brightness. (A) Brightness of different *lux* variants. The *lux* operons schematically shown on the *Right* were expressed from the vector pGEX(-) in DH5 α cells on LB agar plates at 37 °C. Plates were imaged at 37 °C and 22 °C. Error bars represent SDs of six different clones. Nt, N terminus; Ct, C terminus. (B) Temperature curves of *luxCDABE WT* and *ilux*. The bioluminescence signal from DH5 α cells expressing *luxCDABE WT* or *ilux* was measured in suspension at various temperatures. Error bars represent SDs of six independent measurements. (C) Brightness of *ilux* with EYFP-tagged versions of *luxA* and *luxB*. EYFP was introduced into *ilux* pGEX(-) at the N and C termini of *luxA* and *luxB* separated by a glycine-serine linker. Brightness was measured in DH5 α cells on LB agar plates and normalized to the brightness of unlabeled *ilux* at 37 °C. Error bars represent SDs of four different clones.

FMN reductase in mammalian cells, and exogenous addition of the fatty aldehyde (12–15). However, to our knowledge, introduction of mutations in the *luxCDABE* operon to increase the brightness has so far been unsuccessful. Here, we show that bioluminescence from the *lux* operon from *Photobacterium luminescens* expressed in *E. coli* can be substantially enhanced by coexpression of an additional FMN reductase and subsequent error-prone mutagenesis of the complete *lux* operon. The improved *lux* operon dubbed *ilux* can be used to image single *E. coli* cells for extended time periods and to assay cell viability in the presence of different antibiotics.

Results

Engineering and Characterization of the *ilux* Operon. To engineer a bacterial bioluminescence system with improved brightness at 37 °C, we chose the *luxCDABE* operon from *P. luminescens*, as its luciferase has been reported to be more thermostable than *Vibrio harveyi* luciferase (ref. 16 and references therein). The *P. luminescens luxCDABE* operon was cloned into the vector pGEX-6P-1. Details of all primers used for cloning and error-prone PCR are contained in Table S1. Expression in *E. coli* DH5 α cells resulted in only weakly luminescent colonies. Since the function of the fatty acid reductase coded by the *luxC* gene may be affected by the N-terminal GST tag contained in pGEX-6P-1, we expressed the *luxCDABE* operon from a GST-deleted version of this vector, dubbed pGEX(-). This increased the brightness by ~40% at room temperature and ~20-fold at 37 °C (Fig. 1A), suggesting that the activity of the fatty acid reductase is strongly inhibited by the relatively large GST tag at elevated temperature, possibly by inhibiting assembly of the fatty acid reductase complex. In addition, we observed that the bioluminescence signal increases with temperature, yielding two to three times more signal at 37 °C compared with room temperature (22 °C) (Fig. 1A).

To further enhance the bioluminescence intensity, we sought to identify the rate-limiting enzymes of the bioluminescence reaction by cloning a second copy of *luxAB*, *luxCD*, and *luxE* as well as two

different FMN reductases downstream of the *luxCDABE* operon and comparing the brightness with the original construct. The FMN reductase from *E. coli* coded by the *fre* gene and the NADPH-flavin oxidoreductase from *Vibrio campbellii* coded by the *frp* gene resulted in 1.5- and 2.3-fold increases in brightness, respectively (Fig. 1A). This suggested that the endogenous FMN reductase in *E. coli* does not regenerate sufficient amounts of FMNH₂ for maximum levels of bioluminescence. We chose *luxCDABE+frp* pGEX(-) for mutagenesis and performed multiple rounds of error-prone PCR in the *luxAB*, *luxCD*, *luxE*, and *frp* genes. The resulting clones were screened for enhanced luminescence in DH5 α cells on LB agar plates at 37 °C. We identified several mutations in *luxA*, *luxB*, *luxC*, and *frp* that resulted in higher bioluminescence signal, whereas no beneficial mutations in *luxD* and *luxE* were found. The final improved operon called *ilux* contains the mutations listed in Table 1 (complete amino acid sequences of the *ilux* proteins are in Fig. S1). *E. coli* cells expressing the WT *lux* operon (*luxCDABE WT*) and *ilux* exhibited identical bioluminescence emission spectra (Fig. S2). The brightness of *ilux* compared with *luxCDABE WT* was increased not only at 37 °C but also at room temperature (Fig. 1A). Maximum levels of bioluminescence from *E. coli* cells were observed at ~37 °C for both

Table 1. Mutations contained in *ilux*

Gene	Mutations
<i>luxA</i>	K22E, T119A, S178A
<i>luxB</i>	S13P, V121A, N259D
<i>luxC</i>	N10T, N59D, E74D, S256P, M355T, N360D
<i>luxD</i>	—
<i>luxE</i>	—
<i>frp</i>	M213L, R242L, K256R

The listed mutations were introduced by error-prone PCR into the *luxCDABE* operon from *P. luminescens* supplemented with the *frp* gene from *V. campbellii*, resulting in the improved operon *ilux*.

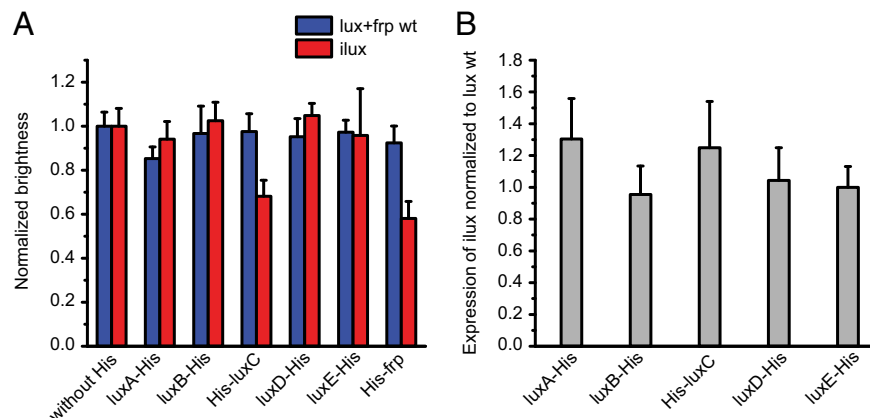


Fig. 2. Brightness and expression of His-tagged proteins in *luxCDABE+frp* and *ilux*. (A) Brightness of *luxCDABE+frp* and *ilux* expressed from pGEX(–) in DH5 α cells. A His tag with a glycine-serine linker was introduced into the indicated proteins in the *lux* operons. Brightness was measured on LB agar plates and normalized to the corresponding nontagged *lux* operon. Error bars represent SDs of 10 different clones. (B) Expression of His-tagged *lux* proteins. Whole-cell lysates of the same clones as in A were analyzed by Western blot. The His signal of each clone was normalized to the housekeeping protein DnaK. Subsequently, the *ilux* signal was normalized to the signal of the same protein in the *luxCDABE+frp* WT operon. Error bars represent SD.

luxCDABE WT and *ilux*, with a slightly broader temperature curve for *ilux* (Fig. 1B). Since we were not able to further improve the cellular signal intensity enabled by the *ilux* operon (“brightness of *ilux*”) by error-prone mutagenesis, we attempted to increase its brightness by bioluminescence resonance energy transfer from the luciferase to an acceptor with high fluorescence quantum yield. For this purpose, we chose the fluorescent protein EYFP [$\Phi_{\text{F}} = 0.61$ (17)] and fused it N- and C-terminally to both the luciferase α and β subunit. However, this did not improve the brightness (Fig. 1C).

To investigate whether the increase in brightness of *ilux* is due to enhanced enzymatic activity or elevated expression of the *lux* proteins, we quantified protein levels by Western blot analysis of cell lysates (Fig. S3). Since antibodies for the *lux* proteins from *P. luminescens* were not available, single proteins in the *luxCDABE* WT and *ilux* operon were expressed with a C-terminal His tag and detected with an anti-His antibody. To control whether the His tag itself affects protein expression, the brightness of cells expressing the His-tagged *lux* operons was compared with the *lux* operon without His tag. The brightness of *ilux luxC*-His and *frp*-His was strongly reduced (Fig. S4), whereas for the other His-tagged proteins the brightness remained comparable with the nontagged operon (Fig. 2A). Therefore, *luxC* and *frp* were instead expressed with an N-terminal His tag, which influenced the brightness less strongly (Fig. 2A). However, the His antibody failed to detect His-*frp* (Fig. S3). Expression of the detectable functional fusion proteins *luxA*-His, *luxB*-His, His-*luxC*, *luxD*-His, and *luxE*-His in both *luxCDABE+frp* and *ilux* was quantified by Western blot (Fig. 2B). Whereas expression of *luxA*-His and His-*luxC* was increased by 30 and 25%, respectively, expression of *luxB*-His, *luxD*-His, and *luxE*-His remained unaffected. Therefore, the increased brightness

of *ilux* seems to be partly due to enhanced expression and partly due to increased activity of the *lux* proteins.

Imaging of Single *E. coli* Cells. To obtain a higher brightness for imaging of single *E. coli* cells, the *ilux* operon was cloned into the vector pQE(–) and expressed in *E. coli* Top10 cells. pQE(–) was generated from pQE30 by deletion of the His tag. Expression of *ilux* from pQE(–) in Top10 cells resulted in a 2.0-fold higher signal at room temperature compared with *ilux* pGEX(–) in DH5 α on LB agar plates (Fig. S5). Although bioluminescence emission was two- to threefold higher at 37 °C, the imaging was performed at room temperature for technical simplicity. Single Top10 cells could already be discriminated after exposure times of only 10–20 s (Fig. 3). Longer exposure times resulted in significantly improved signal-to-noise ratio. A calibration of the camera indicated that 100–200 photons per pixel were detected during a 10-min exposure time, corresponding to 10^3 – 10^4 detected photons per cell per minute.

We compared the brightness of single Top10 cells expressing *ilux* and *luxCDABE* WT. Whereas cells expressing *ilux* could clearly be discriminated after exposure times of 10 min (Fig. 4A), *luxCDABE* WT provided only little signal above background both in the fluorescence and in the bioluminescence images (Fig. 4B). In addition, we compared the brightness of *ilux* with the widely used firefly luciferase (FLuc) (Fig. 4C and D). High concentrations of D-Luciferin of 1 mg/mL were required to visualize the cells, presumably because of low penetration through the bacterial cell wall and membrane. Still, the brightness of FLuc was six to eight times lower than that of *ilux*. In addition, the brightness of FLuc was not constant over time, but single cells sometimes became suddenly much brighter (Fig. 4E). The reason for this is not clear but may be due to increased uptake of the luciferin, since a similar effect was

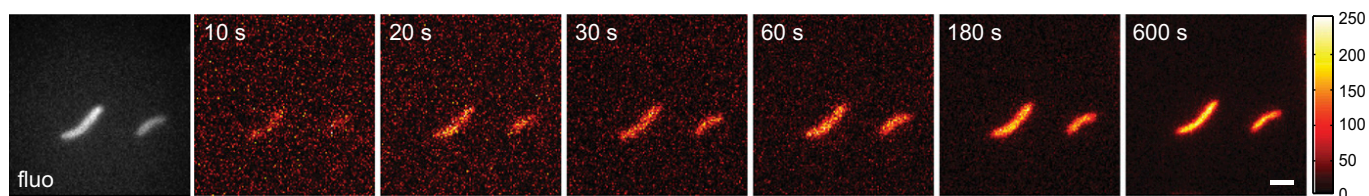


Fig. 3. *E. coli* Top10 cells expressing *ilux* imaged for different exposure times. Bioluminescence images of *E. coli* Top10 cells expressing *ilux* were taken with the indicated exposure times. A fluorescence (fluo) image excited with a 405-nm laser is shown in gray. For the 600-s image, the color bar represents the number of detected photons per pixel. For the other images, the color map was scaled to the minimum and maximum pixel values. (Scale bar: 2 μm .)

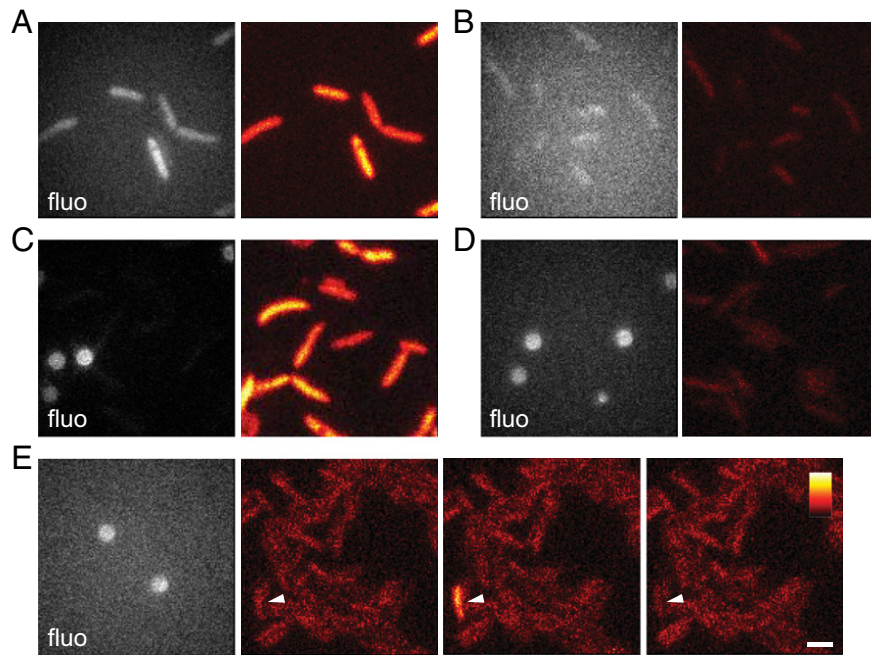


Fig. 4. Comparison of *ilux* with *luxCDABE WT* and FLuc. (A and B) Comparison of brightness of *E. coli* Top10 cells expressing (A) *ilux* or (B) *luxCDABE WT*. The same color map was used for both bioluminescence images. (C and D) Comparison of brightness of *E. coli* Top10 cells expressing (C) *ilux* or (D) FLuc. The same color map was used for both bioluminescence images. (E) *E. coli* Top10 cells expressing FLuc. A cell with a sudden increase and decrease of brightness between three consecutive images is indicated. The same color map was used for all three bioluminescence images. All bioluminescence images were taken with an exposure time of 10 min. Fluorescence (fluo) images excited with a 405-nm laser are shown in gray. For FLuc, fluorescent beads were used for focusing. In the bioluminescence images, the color map was scaled to the minimum and maximum pixel values of A and C and the third column in E. Fig. S6 shows B and D scaled to the minimum and maximum pixel values. (Scale bar: 2 μ m.)

not observed for *ilux*. Together, this shows that *ilux* outperforms both *luxCDABE WT* and FLuc for imaging of single *E. coli* cells due to its superior brightness and stability of the signal.

Next, we aimed at investigating the utility of *ilux* for the observation of single bacteria for extended periods of time. Most cells remained viable over the whole recording time of 12 h and

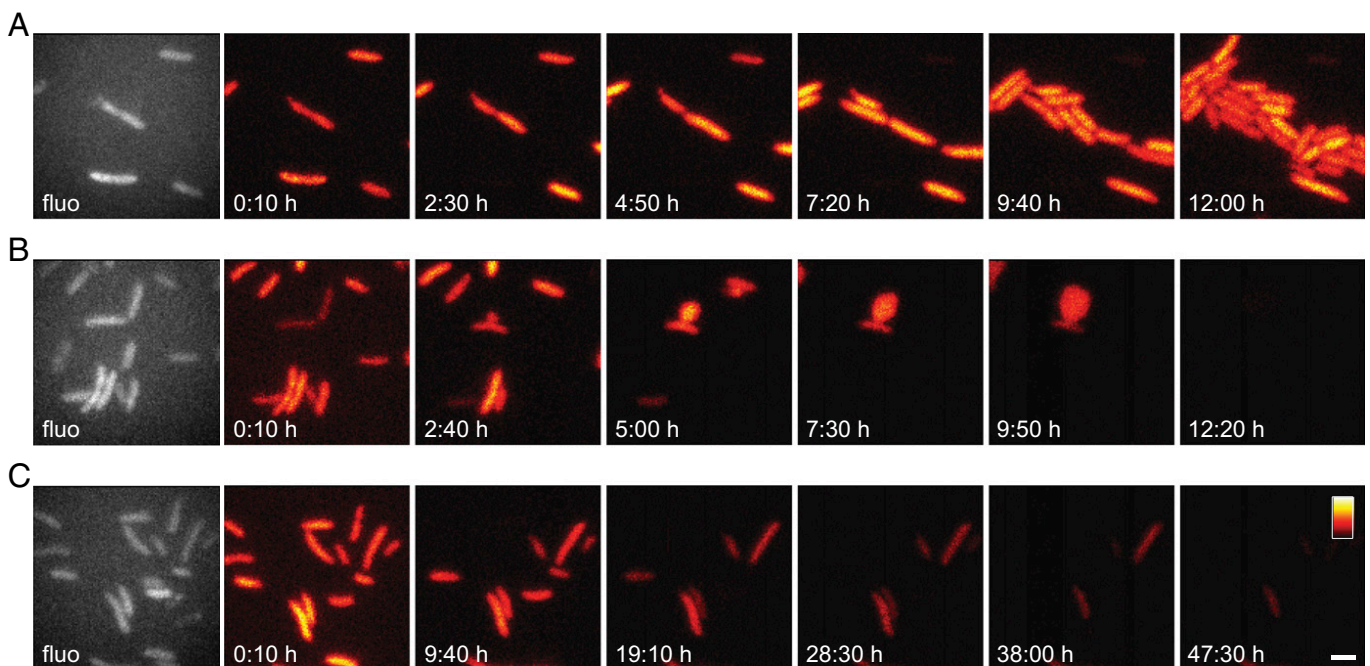


Fig. 5. *E. coli* Top10 cells expressing *ilux* in the presence of different antibiotics. *E. coli* Top10 cells expressing *ilux* were imaged under an LB agar pad containing 50 μ g/mL ampicillin and (A) no additional antibiotics, (B) 100 μ g/mL timentin, or (C) 100 μ g/mL kanamycin. Single images were taken with 10-min exposure time. Fluorescence (fluo) images excited with a 405-nm laser are shown in gray. The same color map was used for all bioluminescence images in each row. Complete time series are shown in Movies S1–S3. (Scale bar: 2 μ m.)

divided several times while maintaining an almost constant bioluminescence signal (Fig. 5A). Subsequently, we investigated the effect of different antibiotics on cell viability. Since continuous supply of ATP and NADPH is required for the regeneration of fatty aldehyde and FMN₂ to keep the bioluminescence reaction ongoing, the signal is expected to disappear on cell death. We imaged Top10 cells in the presence of timentin, a mixture of the β -lactame antibiotic ticarcillin and clavulanic acid. Since pQE(-) contains a β -lactamase resistance marker, cells expressing *ilux* are expected to be resistant to ticarcillin. However, since the β -lactamase is inhibited by clavulanic acid, the cells become susceptible for the cell wall-disrupting effects of ticarcillin and ampicillin. On cell division, this leads to the formation of small holes in the cell wall. As a result, the inner membrane occasionally forms large protrusions due to osmotic pressure (Fig. 5B). This finally leads to cell lysis. After 12 h, all cells in the field of view had died.

The second antibiotic that we examined was kanamycin, an inhibitor of protein synthesis (Fig. 5C). The brightness decreased continuously, consistent with a reduction of protein levels of the *lux* enzymes. Most cells died within the 48-h observation time; nevertheless, bioluminescence was still detectable from a few cells. This shows that, even at high kanamycin concentrations of 100 μ g/mL, cellular metabolism continues for relatively long timespans, although cell division is prevented immediately.

Interestingly, we often observed “blinking” of cells before cell death. The signal from cells that had already disappeared often recovered, sometimes even between two 10- or 3-min frames (Fig. 6A, Fig. S7, and Movies S1–S4). This effect was most pronounced in kanamycin-treated cells, where blinking often occurred

repeatedly (Movies S3 and S4), but it was also occasionally observed in dying cells without additional antibiotics (Movie S1). Blinking was not affected by the presence of ampicillin and was not observed on kanamycin treatment of kanamycin-resistant cells (Movie S5). Blinking cells often continued living for many hours. To determine if blinking results from altered levels of the *ilux* proteins or variations in substrate concentrations, we imaged cells expressing *ilux* with an EYFP-tagged version of *luxB* in the presence of kanamycin. Fluorescence images of EYFP were taken between the bioluminescence images to determine possible alterations of the *luxB*-EYFP protein concentration. Some of the cells that irreversibly lost their bioluminescence signal also exhibited a loss of EYFP fluorescence, whereas other cells retained EYFP fluorescence (Fig. S8A). Blinking cells always retained EYFP fluorescence (Fig. S8B), showing that the protein concentration remains constant. Therefore, we conclude that blinking is caused by rapid fluctuations in metabolite concentrations, most likely ATP or NADPH. To test this hypothesis, we coexpressed the fluorescent ATP biosensor QUEEN-2m with the *ilux* proteins (18). QUEEN-2m fluorescence excited at 405-nm increases with ATP concentration, whereas its fluorescence excited at 490-nm decreases (18). Although QUEEN-2m was designed as a ratiometric ATP sensor, we used its indicator properties at just one excitation wavelength of 491 nm. This allowed us to disentangle the ATP signal from the fluorescence from *ilux*-expressing cells on excitation at 405 nm, while additionally reducing phototoxicity and bioluminescence bleaching. Bioluminescence and fluorescence images were recorded alternately (Fig. 6B). When the bioluminescence signal declined during blinking, the fluorescence signal simultaneously increased. This indicates that the loss of bioluminescence

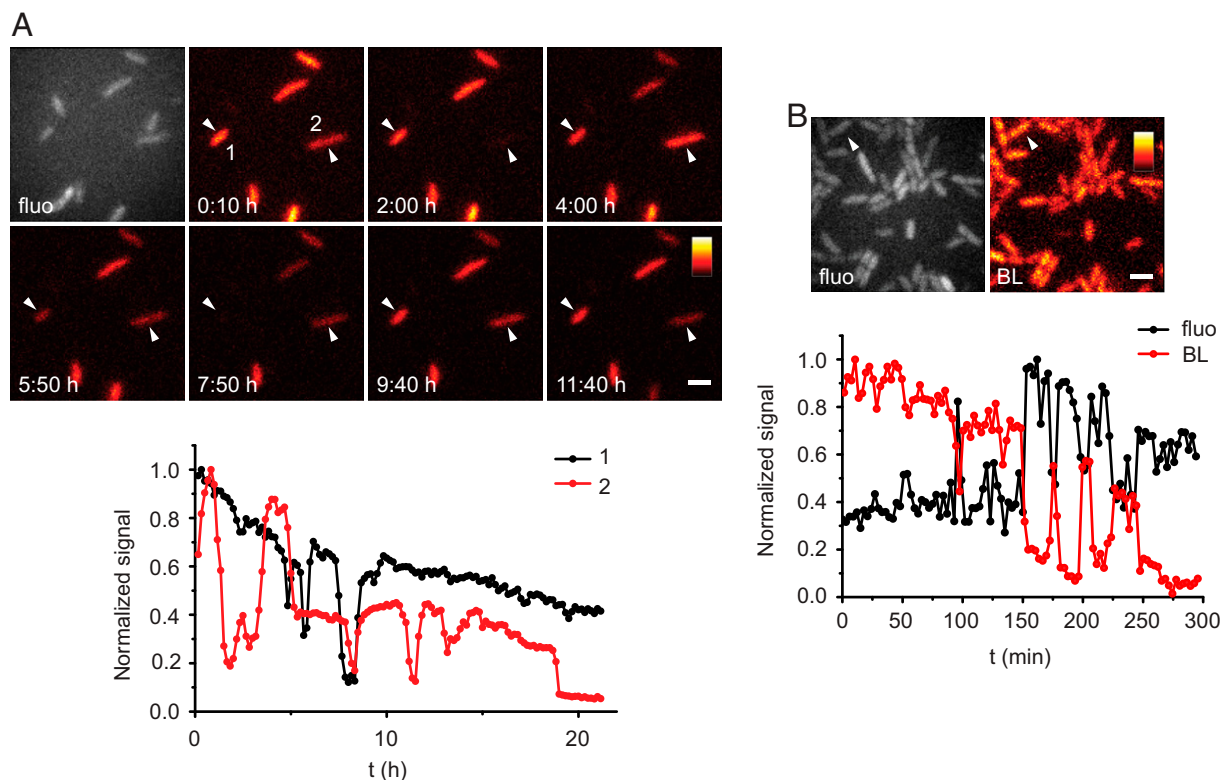


Fig. 6. Blinking of *E. coli* Top10 cells during kanamycin-induced cell death. *E. coli* Top10 cells were imaged under an LB agar pad containing 50 μ g/mL ampicillin and 100 μ g/mL kanamycin. (A) Bioluminescence of *ilux*-expressing cells was imaged with 10-min exposure time. A fluorescence (fluo) image excited with a 405-nm laser is shown in gray. The same color map was used for all bioluminescence images. For the indicated cells, the normalized signal is plotted over time. The complete time series is shown in Movie S4. (B) Bioluminescence (BL) images of Top10 cells expressing *ilux* and the ATP sensor QUEEN-2m were taken with 3-min exposure time. Fluo of QUEEN-2m was excited at 491 nm and recorded between the bioluminescence images. The first fluo and BL images are displayed. For the indicated cell, the normalized signal after subtraction of the background signal outside the cell area is plotted over time. (Scale bars: 2 μ m.)

signal during kanamycin-induced cell death in blinking cells is accompanied by a decrease in ATP concentration.

Discussion and Conclusions

Our results show that bacterial bioluminescence from *E. coli* cells can be enhanced by mutagenesis of the *luxCDABE* genes in combination with introduction of an additional FMN reductase. This allows imaging of single *E. coli* cells with improved spatio-temporal resolution in comparison with previous approaches of single-cell imaging using bacterial bioluminescence (3, 15, 19) without the need of exogenous aldehyde supply. Since the brightness of *ilux* is increased two- to threefold at 37 °C compared with room temperature, heating of the sample during imaging is expected to reduce the necessary recording times further. We have shown that *ilux* can be used to observe processes, such as division and death of single *E. coli* cells, extending the range of applications of bacterial bioluminescence imaging.

The spreading of bacterial antibiotic resistances is becoming an increasing problem for the treatment of human diseases. Therefore, the development of improved and new antibiotics as well as methods to investigate their influence on bacterial viability are urgently required. Taking individual differences between bacteria in the response to antibiotics into account, these methods should preferentially examine bacteria on the single-cell level. A commonly used test for the viability of individual bacteria is the staining with membrane-impermeable dyes, such as propidium iodide (PI), assuming that the dye only enters dead cells with impaired membrane integrity. However, this does not necessarily reflect their metabolic state. Using a FRET-based ATP biosensor, it has been found that not all PI-negative cells of *Mycobacterium smegmatis* exhibit high ATP levels (20), indicating that the membrane may remain intact after cell death. In addition, the authors also observed PI-negative cells with high ATP levels that did not resume growth after antibiotic washout, showing the need to distinguish between membrane integrity, metabolic activity, and the ability of bacteria to divide; *ilux* provides a means for continuous long-term imaging of single bacteria that simultaneously provides information about the metabolic state of the cell.

Unexpectedly, we observed that kanamycin-treated dying cells that lost their bioluminescence can temporarily recover. Given that the protein concentration of *luxB* remains constant during this process and that kanamycin would inhibit the synthesis of new functional proteins, it seems likely that this blinking is not caused by changes in cellular protein levels but rather by altered substrate

concentrations. Fluorescence imaging with the ATP sensor QUEEN-2m showed that the loss of bioluminescence during blinking is correlated with a decrease in the cellular ATP concentration. A possible explanation for this observation is a breakdown of the proton gradient due to the transient formation of membrane defects, which might inhibit ATP synthesis. Indeed, it has been described that aminoglycoside antibiotics can increase cellular permeability by the incorporation of mistranslated membrane proteins (21, 22). Therefore, cell death in kanamycin-treated cells might be the final result of pronounced membrane damage. This would also explain the rapid loss of EYFP fluorescence observed in some kanamycin-treated cells expressing *luxB*-EYFP, as membrane defects might lead to leakage of cellular proteins. Although different explanations for the blinking cannot be excluded, this effect points at interesting applications of *ilux* by providing information about the metabolic activity of the cell.

The independence from exogenous luciferin makes the *lux* system particularly interesting for long-term imaging studies, although its utility has so far been limited by its low brightness compared with other luciferases. Codon-optimized versions of the *lux* proteins have been shown to be functional in eukaryotic cells (13, 14), facilitating observation of bacterial bioluminescence from cell types other than bacteria. Therefore, *ilux* holds promise as a valuable future tool for the observation of mammalian cells as well. In addition, it might be possible to image cellular structures by fusing the luciferase to a protein of interest, allowing its usage in a similar way as fluorescent proteins.

Materials and Methods

Details of the cloning and mutagenesis of the *lux* constructs, measurement of temperature curves, Western blot analysis, and the imaging are described in *SI Materials and Methods*. Briefly, bioluminescence imaging was performed on a custom microscopy setup (Fig. S9) equipped with an oil immersion objective (1.4 N.A.) and an electron multiplying charge-coupled device (EMCCD) camera. The setup additionally contained laser sources for wide-field fluorescence excitation at 405 and 491 nm and a focus lock system for long-term imaging.

ACKNOWLEDGMENTS. We thank Prof. Hiromi Imamura (Kyoto University) for donation of the QUEEN-2m sensor. We thank Dr. Grazvydas Lukinavicius, Torsten Hartmann, and Dr. Waja Wegner for helpful discussions and critical reading of the manuscript and Jasmin Pape for assistance with microscope building. K.C.G. received funding through a graduate scholarship by the Cusanuswerk.

- Haddock SH, Moline MA, Case JF (2010) Bioluminescence in the sea. *Annu Rev Mar Sci* 2:443–493.
- Welsh DK, Noguchi T (2012) Cellular bioluminescence imaging. *Cold Spring Harb Protoc*, 10.1101/pdb.top070607.
- Mihalcescu I, Hsing W, Leibler S (2004) Resilient circadian oscillator revealed in individual cyanobacteria. *Nature* 430:81–85.
- Agulhon C, et al. (2007) Bioluminescent imaging of Ca²⁺ activity reveals spatiotemporal dynamics in glial networks of dark-adapted mouse retina. *J Physiol* 583:945–958.
- Teranishi K, Shimomura O (1997) Solubilizing coelenterazine in water with hydroxypropyl- β -cyclodextrin. *Biosci Biotechnol Biochem* 61:1219–1220.
- Shimomura O, Kishi Y, Inouye S (1993) The relative rate of aequorin regeneration from apoaequorin and coelenterazine analogues. *Biochem J* 296:549–551.
- de Wet JR, Wood KV, DeLuca M, Helinski DR, Subramani S (1987) Firefly luciferase gene: Structure and expression in mammalian cells. *Mol Cell Biol* 7:725–737.
- Inoue Y, et al. (2011) Gaussia luciferase for bioluminescence tumor monitoring in comparison with firefly luciferase. *Mol Imaging* 10:377–385.
- Stacer AC, et al. (2013) NanoLuc reporter for dual luciferase imaging in living animals. *Mol Imaging* 12:1–13.
- Zhao H, et al. (2004) Characterization of coelenterazine analogs for measurements of Renilla luciferase activity in live cells and living animals. *Mol Imaging* 3:43–54.
- Close DM, et al. (2011) Comparison of human optimized bacterial luciferase, firefly luciferase, and green fluorescent protein for continuous imaging of cell culture and animal models. *J Biomed Opt* 16:047003.
- Yagur-Kroll S, Belkin S (2011) Upgrading bioluminescent bacterial bioreporter performance by splitting the *lux* operon. *Anal Bioanal Chem* 400:1071–1082.
- Close DM, et al. (2010) Autonomous bioluminescent expression of the bacterial luciferase gene cassette (*lux*) in a mammalian cell line. *PLoS One* 5:e12441.
- Xu T, Ripp S, Saylor GS, Close DM (2014) Expression of a humanized viral 2A-mediated *lux* operon efficiently generates autonomous bioluminescence in human cells. *PLoS One* 9:e96347.
- Sternberg C, Eberl L, Poulsen LK, Molin S (1997) Detection of bioluminescence from individual bacterial cells: A comparison of two different low-light imaging systems. *J Biolumin Chemilumin* 12:7–13.
- Westerlund-Karlsson A, Saviranta P, Karp M (2002) Generation of thermostable monomeric luciferases from *Photobacterium luminescens*. *Biochem Biophys Res Commun* 296:1072–1076.
- Patterson G, Day RN, Piston D (2001) Fluorescent protein spectra. *J Cell Sci* 114:837–838.
- Yaginuma H, et al. (2014) Diversity in ATP concentrations in a single bacterial cell population revealed by quantitative single-cell imaging. *Sci Rep* 4:6522.
- Phiefer CB, Palmer RJJ, Jr, White DC (1999) Comparison of relative photon flux from single cells of the bioluminescent marine bacteria *Vibrio fischeri* and *Vibrio harveyi* using photon-counting microscopy. *Luminescence* 14:147–151.
- Maglica Ž, Özdemir E, McKinney JD (2015) Single-cell tracking reveals antibiotic-induced changes in mycobacterial energy metabolism. *MBio* 6:e02236–14.
- Davis BD, Chen LL, Tai PC (1986) Misread protein creates membrane channels: An essential step in the bactericidal action of aminoglycosides. *Proc Natl Acad Sci USA* 83:6164–6168.
- Kohanski MA, Dwyer DJ, Collins JJ (2010) How antibiotics kill bacteria: From targets to networks. *Nat Rev Microbiol* 8:423–435.